Supplementary Material: Order and symmetry-breaking in the fluctuations of driven systems

N. Tizón-Escamilla,[1] C. Pérez-Espigares,[2,3] P.L. Garrido,[1] and P.I. Hurtado[1,*]

[1] *Departamento de Electromagnetismo y Física de la Materia, and Institute Carlos I for Theoretical and Computational Physics, Universidad de Granada, Granada 18071, Spain*
[2] *University of Modena and Reggio Emilia, via G. Campi 213/b, 41125 Modena, Italy*
[3] *School of Physics and Astronomy, University of Nottingham, Nottingham, NG7 2RD, UK*

(Dated: July 24, 2017)

I. DYNAMIC PHASE TRANSITIONS IN THE CURRENT VECTOR STATISTICS FROM MACROSCOPIC FLUCTUATION THEORY

In this section we analyze the equations of macroscopic fluctuation theory (MFT) for the current vector statistics of arbitrary driven diffusive systems, with special emphasis on the MFT predictions regarding the existence and nature of dynamic phase transitions (DPTs) in some regimes of current fluctuations. In particular, we consider a broad class of d-dimensional anisotropic driven diffusive systems characterized by a locally-conserved density field $\rho(\mathbf{r},t)$ which evolves in time according to the following fluctuating hydrodynamics equation [1–3]

$$\partial_t \rho(\mathbf{r},t) + \boldsymbol{\nabla}\cdot\left(-\hat{D}(\rho)\boldsymbol{\nabla}\rho(\mathbf{r},t) + \hat{\sigma}(\rho)\mathbf{E} + \boldsymbol{\xi}(\mathbf{r},t)\right) = 0\,, \tag{1}$$

with $\mathbf{E}$ the external field driving the system out of equilibrium and $\mathbf{r}\in\Lambda\equiv[0,1]^d$. The field $\mathbf{j}(\mathbf{r},t)\equiv-\hat{D}(\rho)\boldsymbol{\nabla}\rho(\mathbf{r},t)+\hat{\sigma}(\rho)\mathbf{E}+\boldsymbol{\xi}(\mathbf{r},t)$ is the fluctuating current, with $\hat{D}(\rho)\equiv D(\rho)\hat{\mathcal{A}}$ and $\hat{\sigma}(\rho)=\sigma(\rho)\hat{\mathcal{A}}$ the diffusivity and mobility matrices, respectively, and $\hat{\mathcal{A}}$ a diagonal anisotropy matrix with components $\hat{\mathcal{A}}_{\alpha\beta}=a_\alpha\delta_{\alpha\beta}$, $\alpha,\beta\in[1,d]$. The noise term $\boldsymbol{\xi}(\mathbf{r},t)$ is Gaussian and white with zero average, $\langle\boldsymbol{\xi}(\mathbf{r},t)\rangle=0$, and variance

$$\langle\xi_\alpha(\mathbf{r},t)\xi_\beta(\mathbf{r}',t')\rangle = L^{-d}\sigma(\rho)a_\alpha\delta_{\alpha\beta}\delta(\mathbf{r}-\mathbf{r}')\delta(t-t')\,, \tag{2}$$

with L the system size in natural units. This (conserved) noise term accounts for the many fast microscopic degrees of freedom which are averaged out in the coarse-graining procedure resulting in Eq. (1). The diffusion and mobility transport matrices fully characterize the macroscopic fluctuation properties of the model at hand, being related via a local Einstein relation $\hat{D}(\rho)=f_0''(\rho)\hat{\sigma}(\rho)$, with $f_0(\rho)$ the *equilibrium* free energy of the system. To completely define the problem, the evolution equation (1) must be supplemented with appropriate boundary conditions, which in this case are simply periodic along all d directions.

Now, starting from the Fokker-Planck description of the Langevin equation (1) and using a path integral formalism, the probability of observing a given trajectory $\{\rho(\mathbf{r},t),\mathbf{j}(\mathbf{r},t)\}_0^\tau$ of duration τ for the density and current fields can be written as [1]

$$\mathrm{P}\left(\{\rho,\mathbf{j}\}_0^\tau\right) \asymp \exp\Big(+L^d I_\tau\left[\rho,\mathbf{j}\right]\Big)\,, \tag{3}$$

where the symbol "$\asymp$" stands for asymptotic logarithmic equality, i.e.

$$\lim_{L\to\infty}\frac{1}{L^d}\ln\mathrm{P}\left(\{\rho,\mathbf{j}\}_0^\tau\right) = I_\tau\left[\rho,\mathbf{j}\right]\,. \tag{4}$$

The action of Eq. (3) is

$$I_\tau\left[\rho,\mathbf{j}\right] = -\int_0^\tau dt\int_\Lambda d\mathbf{r}\,\frac{1}{2\sigma(\rho)}\left(\mathbf{j}+D(\rho)\hat{\mathcal{A}}\boldsymbol{\nabla}\rho-\sigma(\rho)\hat{\mathcal{A}}\mathbf{E}\right)\cdot\hat{\mathcal{A}}^{-1}\left(\mathbf{j}+D(\rho)\hat{\mathcal{A}}\boldsymbol{\nabla}\rho-\sigma(\rho)\hat{\mathcal{A}}\mathbf{E}\right)\,, \tag{5}$$

where the fields $\rho(\mathbf{r},t)$ and $\mathbf{j}(\mathbf{r},t)$ are coupled via the continuity equation, see Eq. (1),

$$\partial_t\rho(\mathbf{r},t)+\boldsymbol{\nabla}\cdot\mathbf{j}(\mathbf{r},t)=0\,. \tag{6}$$

* phurtado@onsager.ugr.es

For any other trajectory not obeying (6), $I_\tau\,[\rho,\mathbf{j}] \to -\infty$. Moreover, the system of interest is isolated so that the total mass is conserved,

$$\rho_0 = \int_\Lambda d\mathbf{r}\,\rho(\mathbf{r},t)\,. \tag{7}$$

The probability $\mathrm{P}_\tau(\mathbf{q})$ of observing a space- and time-averaged empirical current *vector* $\mathbf{q}$, defined as

$$\mathbf{q} = \frac{1}{\tau}\int_0^\tau dt \int_\Lambda d\mathbf{r}\,\mathbf{j}(\mathbf{r},t)\,, \tag{8}$$

scales for long times as $\mathrm{P}_\tau(\mathbf{q}) \asymp \exp[+\tau L^d G(\mathbf{q})]$, and the current large deviation function (LDF) $G(\mathbf{q})$ can be related to $I_\tau[\rho,\mathbf{j}]$ via a simple saddle-point calculation in the long-time limit,

$$G(\mathbf{q}) = \lim_{\tau\to\infty}\frac{1}{\tau}\max_{\{\rho,\mathbf{j}\}_0^\tau} I_\tau[\rho,\mathbf{j}]\,, \tag{9}$$

subject to constraints (6), (7) and (8). The density and current fields solution of this variational problem, denoted here as $\rho_{\mathbf{q}}(\mathbf{r},t)$ and $\mathbf{j}_{\mathbf{q}}(\mathbf{r},t)$, correspond to the optimal path the system follows in mesoscopic phase space to sustain a long-time current fluctuation $\mathbf{q}$. This path may be in general time-dependent, and the associated general variational problem is remarkably hard.

This problem becomes simpler however in different limiting cases. For instance, in the steady state the system exhibits translation symmetry with an homogeneous stationary density profile $\rho_{\mathrm{st}}(\mathbf{r}) = \rho_0$ and a constant average current $\mathbf{j}_{\mathrm{st}}(\mathbf{r}) = \langle\mathbf{q}\rangle = \sigma_0\hat{\mathcal{A}}\mathbf{E}$, where we have defined $\sigma_0 \equiv \sigma(\rho_0)$. Now, one can argue that small fluctuations of the empirical current $\mathbf{q}$ away from the average behavior $\langle\mathbf{q}\rangle$ will typically result from weakly-correlated local events in different parts of the system which add up incoherently to yield the desired $\mathbf{q}$, so the optimal density field associated to these small fluctuations still corresponds to the homogeneous, stationary one [9, 11], i.e. $\rho_{\mathbf{q}}(\mathbf{r},t) = \rho_0$ for $|\mathbf{q}-\langle\mathbf{q}\rangle| \ll 1$, while the optimal current field is constant, $\mathbf{j}_{\mathbf{q}}(\mathbf{r},t) = \mathbf{q}$, leading to a quadratic current LDF corresponding to Gaussian current statistics,

$$G_{\mathrm{G}}(\mathbf{q}) = -\frac{1}{2\sigma_0}\left(\mathbf{q}-\sigma_0\hat{\mathcal{A}}\mathbf{E}\right)\cdot\hat{\mathcal{A}}^{-1}\left(\mathbf{q}-\sigma_0\hat{\mathcal{A}}\mathbf{E}\right)\,, \tag{10}$$

as indeed corroborated in our simulations for a broad range of $\mathbf{q}$'s. As an interesting by-product, note that current fluctuations in this Gaussian regime obey an anisotropic version of the Isometric Fluctuation Theorem [4–6], which links in simple terms the probability of two different but $\hat{\mathcal{A}}$-isometric current vector fluctuations. In particular,

$$\lim_{\tau\to\infty}\frac{1}{\tau L^d}\ln\left[\frac{P_\tau(\mathbf{q})}{P_\tau(\mathbf{q}')}\right] = \mathbf{E}\cdot(\mathbf{q}-\mathbf{q}')\,, \tag{11}$$

$\forall\mathbf{q},\mathbf{q}'$ in the Gaussian regime such that $\mathbf{q}\cdot\hat{\mathcal{A}}\mathbf{q} = \mathbf{q}'\cdot\hat{\mathcal{A}}\mathbf{q}'$.

Interestingly, the above ansatz with the associated *flat* profiles remains a solution of the full variational problem $\forall\mathbf{q}$, but the question remains as to whether other solutions with more complex spatiotemporal structure may yield a better maximizer of the MFT action (9) for currents. To address this question, we now perturb the above flat solution with small but otherwise arbitrary functions of space and time, and study the local stability of the homogeneous solution against such perturbations. In particular, we ask whether the perturbed fields yield in some case a larger $G(\mathbf{q})$. With this aim in mind, we write

$$\bar{\rho}(\mathbf{r},t) = \rho_0 + \delta\rho(\mathbf{r},t), \qquad \bar{\mathbf{j}}(\mathbf{r},t) = \mathbf{q} + \delta\mathbf{j}(\mathbf{r},t)\,, \tag{12}$$

where both $\bar{\rho}(\mathbf{r},t)$ and $\bar{\mathbf{j}}(\mathbf{r},t)$ remain constrained by Eqs. (6), (7) and (8). Inserting these expressions in Eq. (9) and expanding to second order in the perturbations, we obtain the leading correction to the quadratic form $G_{\mathrm{G}}(\mathbf{q})$ of Eq. (10) (termed here $O2$)

$$O2 = -\frac{1}{2\tau}\int_0^\tau dt\int_\Lambda d\mathbf{r}\left\{A(\rho_0,\mathbf{q})\delta\rho^2 + \boldsymbol{\nabla}\delta\rho\cdot\hat{B}(\rho_0)\boldsymbol{\nabla}\delta\rho + \delta\mathbf{j}\cdot\hat{C}(\rho_0)\delta\mathbf{j} + \delta\mathbf{j}\cdot\mathbf{F}(\rho_0,\mathbf{q})\delta\rho\right\}\,, \tag{13}$$

where we have defined

$$A(\rho_0,\mathbf{q}) = \left(\frac{\sigma_0'^2}{\sigma_0^3} - \frac{\sigma_0''}{2\sigma_0^2}\right)\mathbf{q}\cdot\hat{\mathcal{A}}^{-1}\mathbf{q} + \sigma_0''\mathbf{E}\cdot\hat{\mathcal{A}}\mathbf{E}, \quad \hat{B}(\rho_0) = \frac{D_0^2}{\sigma_0}\hat{\mathcal{A}}, \quad \hat{C}(\rho_0) = \frac{\hat{\mathcal{A}}^{-1}}{\sigma_0}, \quad \mathbf{F}(\rho_0,\mathbf{q}) = -\frac{\sigma_0'}{\sigma_0^2}\hat{\mathcal{A}}^{-1}\mathbf{q}\,, \tag{14}$$

with $'$ denoting derivative with respect to the argument, and $D_0 \equiv D(\rho_0)$. We next expand the perturbations $\delta\rho(\mathbf{r},t)$ and $\delta\mathbf{j}(\mathbf{r},t)$ in Fourier series, taking advantage of the spatial periodic boundary conditions, and imposing explicitly along the way the constraints (6), (7) and (8). For simplicity we particularize hereafter our results for dimension two, $d=2$, though the generalization to arbitrary d is straightforward. In this way, perturbations take the form

$$\delta\rho(\mathbf{r},t) = \sum_{\nu} \frac{1}{\nu}\Big[-\nabla\cdot\boldsymbol{\gamma}_{1,\nu}(\mathbf{r})\sin(\nu t) + \nabla\cdot\boldsymbol{\gamma}_{2,\nu}(\mathbf{r})\cos(\nu t)\Big], \tag{15}$$

$$\delta\mathbf{j}(\mathbf{r},t) = \sum_{\nu} \Big[\boldsymbol{\gamma}_{1,\nu}(\mathbf{r})\cos(\nu t) + \boldsymbol{\gamma}_{2,\nu}(\mathbf{r})\sin(\nu t)\Big], \tag{16}$$

where the first equation follows from the second expansion after imposing the continuity constraint (6), with

$$\boldsymbol{\gamma}_{1,\nu}(\mathbf{r}) = \frac{1}{4}\mathbf{a}_{\nu 00} + \frac{1}{2}\sum_{k_1\neq 0}(\mathbf{a}_{\nu k_1 0}\cos k_1 x + \mathbf{c}_{\nu k_1 0}\sin k_1 x) + \frac{1}{2}\sum_{k_2\neq 0}(\mathbf{a}_{\nu 0 k_2}\cos k_2 y + \mathbf{b}_{\nu 0 k_2}\sin k_2 y) + \tag{17}$$
$$+ \sum_{k_1,k_2\neq 0}(\mathbf{a}_{\nu k_1 k_2}\cos k_1 x\cos k_2 y + \mathbf{b}_{\nu k_1 k_2}\cos k_1 x\sin k_2 y + \mathbf{c}_{\nu k_1 k_2}\sin k_1 x\cos k_2 y + \mathbf{d}_{\nu k_1 k_2}\sin k_1 x\sin k_2 y)$$

$$\boldsymbol{\gamma}_{2,\nu}(\mathbf{r}) = \frac{1}{4}\mathbf{s}_{\nu 00} + \frac{1}{2}\sum_{k_1\neq 0}(\mathbf{s}_{\nu k_1 0}\cos k_1 x + \mathbf{u}_{\nu k_1 0}\sin k_1 x) + \frac{1}{2}\sum_{k_2\neq 0}(\mathbf{s}_{\nu 0 k_2}\cos k_2 y + \mathbf{t}_{\nu 0 k_2}\sin k_2 y) + \tag{18}$$
$$+ \sum_{k_1,k_2\neq 0}(\mathbf{s}_{\nu k_1 k_2}\cos k_1 x\cos k_2 y + \mathbf{t}_{\nu k_1 k_2}\cos k_1 x\sin k_2 y + \mathbf{u}_{\nu k_1 k_2}\sin k_1 x\cos k_2 y + \mathbf{v}_{\nu k_1 k_2}\sin k_1 x\sin k_2 y)$$

where $\mathbf{a}_{\nu ij}$, $\mathbf{b}_{\nu ij}$, $\mathbf{c}_{\nu ij}$, $\mathbf{d}_{\nu ij}$, $\mathbf{s}_{\nu ij}$, $\mathbf{t}_{\nu ij}$, $\mathbf{u}_{\nu ij}$, $\mathbf{v}_{\nu ij}$ are the coefficients of the Fourier series. Note that the previous expansion has been divided into first the only-temporal modes, then all $1+1$ spatiotemporal modes along each direction of space, and finally the fully $2+1$ spatiotemporal modes. The $O2$ correction (13) is of course a quadratic form of the perturbations with constant coefficients, so the different Fourier modes decouple simplifying the problem. In this way the stability analysis melts down as usual to an eigenvalue problem, which in this case splits into different problems for only temporal modes, spatiotemporal modes with structure along just one dimension, x or y, and $2d$ spatiotemporal modes, which can be analyzed separately. This straightforward but lengthy calculation leads to the following conclusion: the flat solution corresponding to Gaussian current statistics remains stable (i.e. the $O2$ correction is negative) whenever the following conditions hold,

$$\begin{aligned} a_{\min}k_n^2\frac{D_0^2}{\sigma_0} + H(\mathbf{E},\mathbf{q}) &> 0 \\ a_{\max}k_m^2\frac{D_0^2}{\sigma_0} + H(\mathbf{E},\mathbf{q}) &> 0 \\ \left(a_{\min}k_n^2 + a_{\max}k_m^2\right)\frac{D_0^2}{\sigma_0} + H(\mathbf{E},\mathbf{q}) &> 0, \end{aligned} \tag{19}$$

with $k_n = 2\pi n$ and $k_m = 2\pi m$ the different spatial modes associated to each perturbation along either direction, $a_{\min} = \min\{a_\alpha, \alpha\in[1,d]\}$ and $a_{\max} = \max\{a_\alpha, \alpha\in[1,d]\}$, and

$$H(\mathbf{E},\mathbf{q}) = \frac{\sigma_0''}{2}\left(\mathbf{E}\cdot\hat{\mathcal{A}}\mathbf{E} - \sigma_0^{-2}\mathbf{q}\cdot\hat{\mathcal{A}}^{-1}\mathbf{q}\right) \tag{20}$$

A number of important conclusions can be directly derived from this set of conditions, namely:

(i) The first mode to become unstable (if any) is always the fundamental mode $k_1 = 2\pi$.

(ii) For any value of the anisotropy, the first perturbations to become unstable are those with structure along one spatial dimension, x or y.

(iii) For anisotropic systems, $a_{\min} < a_{\max}$, the leading unstable perturbation has structure in the direction of minimum anisotropy.

(iv) For isotropic systems, $a_{\min} = a_{\max} \equiv a$, both one-dimensional perturbations trigger the instability of the flat solution at the same point. In this case, the orientation of the current vector $\mathbf{q}$ determines the most probable profile immediately after the instability kicks in, with structure only along the x- or y-direction, as dictated by the term proportional to $\mathbf{F}(\rho_0,\mathbf{q})$ in the $O2$ correction, see Eq. (13).

Therefore there exists a line of critical values for the current $\mathbf{q}_c$ at which the instability appears, given by

$$\mathbf{q}_c \cdot \hat{\mathcal{A}}^{-1}\mathbf{q}_c = \sigma_0^2 \left(\mathbf{E}\cdot\hat{\mathcal{A}}\mathbf{E} + 8\pi^2 a_{\min}\frac{D_0^2}{\sigma_0\sigma_0''}\right) \equiv \sigma_0^2\Xi_c\,. \tag{21}$$

For systems with $\sigma_0'' > 0$ (as e.g. the Kipnis-Marchioro-Presutti model of heat transport [3, 4, 7]), the instability appears always, regardless of the value of the external field (even for $\mathbf{E}=0$), separating a regime of Gaussian current statistics for $\mathbf{q}\cdot\hat{\mathcal{A}}^{-1}\mathbf{q} \leq \sigma_0^2\Xi_c$ and a non-Gaussian region for $\mathbf{q}\cdot\hat{\mathcal{A}}^{-1}\mathbf{q} > \sigma_0^2\Xi_c$. On the other hand, for systems with $\sigma_0'' < 0$ (as the weakly asymmetric simple exclusion process –WASEP– studied in this paper [8–10]) a line of critical values of the external field exists, defined by

$$\mathbf{E}_c\cdot\hat{\mathcal{A}}\mathbf{E}_c = 8\pi^2 a_{\min}\frac{D_0^2}{\sigma_0|\sigma_0''|} \equiv |\Sigma_c|\,. \tag{22}$$

beyond which the instability appears, $\mathbf{E}\cdot\hat{\mathcal{A}}\mathbf{E} \geq |\Sigma_c|$. In this strong field case, Gaussian statistics are expected for all currents except for a region around $\mathbf{q}=0$, defined by $\mathbf{q}\cdot\hat{\mathcal{A}}^{-1}\mathbf{q} \leq \sigma_0^2\Xi_c$, where current fluctuations are non-Gaussian. For weak external fields, $\mathbf{E}\cdot\hat{\mathcal{A}}\mathbf{E} < |\Sigma_c|$, only Gaussian statistics are observed.

Whenever the instability emerges, the first two frequencies to become unstable are $\nu_c^{\pm} = \pm 2\pi q_{\|}\sigma_0'/\sigma_0$, with $q_{\|}$ the component of the current vector along the direction of structure formation (that we denote here as $x_{\|}$). Considering that the first unstable spatial mode correspond to $k_{\perp}=0$, $k_{\|}=2\pi$, the resulting leading perturbations simplify to

$$\delta\rho_{\pm}(\mathbf{r},t) = \frac{\pi}{\nu_c^{\pm}}\left(a^{(2)}_{\nu_c^{\pm}01}\sin 2\pi x_{\|} - b^{(2)}_{\nu_c^{\pm}01}\cos 2\pi x_{\|}\right)\sin\nu_c^{\pm}t + \left(-s^{(2)}_{\nu_c^{\pm}01}\sin 2\pi x_{\|} + t^{(2)}_{\nu_c^{\pm}01}\cos 2\pi x_{\|}\right)\cos\nu_c^{\pm}t \tag{23}$$

$$\delta\mathbf{j}_{\pm}(\mathbf{r},t) = \frac{1}{2}\left(\mathbf{a}_{\nu_c^{\pm}01}\cos 2\pi x_{\|} + \mathbf{b}_{\nu_c^{\pm}01}\sin 2\pi x_{\|}\right)\cos\nu_c^{\pm}t + \left(\mathbf{s}_{\nu_c^{\pm}01}\cos 2\pi x_{\|} + \mathbf{t}_{\nu_c^{\pm}01}\sin 2\pi x_{\|}\right)\sin\nu_c^{\pm}t \tag{24}$$

with $\mathbf{a}_{\nu_c^{\pm}01} = (a^{(1)}_{\nu_c^{\pm}01}, a^{(2)}_{\nu_c^{\pm}02})$, $\mathbf{b}_{\nu_c^{\pm}01} = (b^{(1)}_{\nu_c^{\pm}01}, b^{(2)}_{\nu_c^{\pm}02})$, $\mathbf{s}_{\nu_c^{\pm}01} = (s^{(1)}_{\nu_c^{\pm}01}, s^{(2)}_{\nu_c^{\pm}02})$, $\mathbf{t}_{\nu_c^{\pm}01} = (t^{(1)}_{\nu_c^{\pm}01}, t^{(2)}_{\nu_c^{\pm}02})$ the coefficients of the Fourier series corresponding to that mode. Introducing these perturbations in (13) and imposing $O2>0$ [9], we arrive at a relation between the different coefficients, $a^{(2)}_{01} = \pm t^{(2)}_{01}$, $b^{(2)}_{01} = \mp s^{(2)}_{01}$ for $\nu_c^{\pm}$. As a result, the dominant perturbation of the density profile once the instability is triggered takes the form of a one-dimensional traveling wave

$$\delta\rho(x_{\|},t) = A\sin\left[2\pi\left(x_{\|} - x_{\|}^0 - \frac{q_{\|}\sigma_0'}{\sigma_0}t\right)\right], \tag{25}$$

with A and $x_{\|}^0$ two arbitrary constants.

With this result in mind, we consider now that the relevant density fields well below the instability conserve a traveling-wave structure, i.e. $\rho(\mathbf{r},t) \equiv \omega(\mathbf{r}-\mathbf{v}t)$, with $\mathbf{v}$ some velocity vector to be determined in the variational problem. Taking now into account the continuity constraint Eq. (6) we have that $\boldsymbol{\nabla}_{\mathbf{r}'}\cdot\mathbf{j}(\mathbf{r}') = \mathbf{v}\cdot\boldsymbol{\nabla}_{\mathbf{r}'}\omega(\mathbf{r}')$, with the definition $\mathbf{r}' = \mathbf{r}-\mathbf{v}t$. Integrating the previous expression leads to

$$\mathbf{j}(\mathbf{r},t) = \mathbf{v}\omega(\mathbf{r}-\mathbf{v}t) + \boldsymbol{\Phi}(\mathbf{r}-\mathbf{v}t)\,, \tag{26}$$

where $\boldsymbol{\Phi}(\mathbf{r}-\mathbf{v}t)$ is an arbitrary divergence-free vector field. To explicitly account for the constraint (8) on the empirical current, we now split the field $\boldsymbol{\Phi}$ into two terms, $\boldsymbol{\Phi}(\mathbf{r}-\mathbf{v}t) = \mathbf{k} + \boldsymbol{\phi}(\mathbf{r}-\mathbf{v}t)$, where $\mathbf{k} = \mathbf{q} - \mathbf{v}\rho_0$ is a constant vector fixed by constaints (7) and (8), and $\boldsymbol{\phi}(\mathbf{r}-\mathbf{v}t)$ is now an arbitrary divergence-free field with zero integral, see Eqs. (32)-(33) below, defining another degree of freedom (a sort of *gauge field*) to be determined in the variational problem. The resulting traveling-wave form of the current field is

$$\mathbf{j}(\mathbf{r},t) = \mathbf{q} - \mathbf{v}\left[\rho_0 - \omega(\mathbf{r}-\mathbf{v}t)\right] + \boldsymbol{\phi}(\mathbf{r}-\mathbf{v}t)\,. \tag{27}$$

Interestingly, the system uses this kind of *gauge freedom* to optimize a given current fluctuation in the symmetry-broken phase, selecting among all possible *gauges* a particular, non-trivial one which maximizes the probability of this event. This sort of gauge freedom is precisely the key feature responsible of the richness of the fluctuation phase diagram for $d>1$.

In this way, under the above traveling-wave assumptions, the current LDF of Eq. (9) can now be written, after a change of variables $(\mathbf{r}-\mathbf{v}t)\to\mathbf{r}$, as

$$G(\mathbf{q}) = -\min_{\omega,\boldsymbol{\phi},\mathbf{v}}\int_{\Lambda} d\mathbf{r}\,\mathcal{G}_{\mathbf{q}}(\omega,\boldsymbol{\phi},\mathbf{v}), \tag{28}$$

with the definitions

$$\mathcal{G}_{\mathbf{q}}(\omega,\boldsymbol{\phi},\mathbf{v}) \equiv \frac{1}{2\sigma(\omega)}\boldsymbol{\mathcal{J}}_{\mathbf{q}}(\omega,\boldsymbol{\phi},\mathbf{v})\cdot\hat{\mathcal{A}}^{-1}\boldsymbol{\mathcal{J}}_{\mathbf{q}}(\omega,\boldsymbol{\phi},\mathbf{v}), \tag{29}$$

$$\boldsymbol{\mathcal{J}}_{\mathbf{q}}(\omega,\boldsymbol{\phi},\mathbf{v}) \equiv \mathbf{q}-\mathbf{v}\left[\rho_0-\omega(\mathbf{r})\right]+\boldsymbol{\phi}(\mathbf{r})+D(\omega)\hat{\mathcal{A}}\boldsymbol{\nabla}\omega-\sigma(\omega)\hat{\mathcal{A}}\mathbf{E}\,, \tag{30}$$

and with the additional constraints

$$\rho_0 = \int_\Lambda \omega(\mathbf{r})\,d\mathbf{r} \tag{31}$$

$$\int_\Lambda \boldsymbol{\phi}(\mathbf{r})\,d\mathbf{r} = 0 \tag{32}$$

$$\boldsymbol{\nabla}\cdot\boldsymbol{\phi}(\mathbf{r}) = 0 \tag{33}$$

To account for these constraints, we employ the method of Lagrange multipliers. In particular, we write

$$G(\mathbf{q}) = -\min_{\substack{\omega,\boldsymbol{\phi},\mathbf{v}\\ \zeta,\boldsymbol{\kappa},\Psi}}\int_\Lambda d\mathbf{r}\,\tilde{\mathcal{G}}_{\mathbf{q}}(\omega,\boldsymbol{\phi},\mathbf{v},\zeta,\boldsymbol{\kappa},\Psi), \tag{34}$$

where the modified functional to minimize is

$$\tilde{\mathcal{G}}_{\mathbf{q}}(\omega,\boldsymbol{\phi},\mathbf{v},\zeta,\boldsymbol{\kappa},\Psi) \equiv \mathcal{G}_{\mathbf{q}}(\omega,\boldsymbol{\phi},\mathbf{v})+\zeta\left[\rho_0-\omega(\mathbf{r})\right]+\boldsymbol{\kappa}\cdot\boldsymbol{\phi}(\mathbf{r})+\Psi(\mathbf{r})\boldsymbol{\nabla}\cdot\boldsymbol{\phi}(\mathbf{r})\,, \tag{35}$$

and ζ, $\boldsymbol{\kappa}$ and $\Psi(\mathbf{r})$ are the Lagrange multipliers associated to the constraints (31), (32) and (33), respectively. Standard variational calculus shows now that the optimal fields and velocity solution of this complex variational problem, denoted as $\omega_{\mathbf{q}}(\mathbf{r})$, $\boldsymbol{\phi}_{\mathbf{q}}(\mathbf{r})$, and $\mathbf{v}_{\mathbf{q}}$, obey the following system of coupled equations,

$$\left[\frac{\mathbf{v}_{\mathbf{q}}}{\sigma(\omega_{\mathbf{q}})}-\frac{\sigma'(\omega_{\mathbf{q}})}{2\sigma(\omega_{\mathbf{q}})^2}\mathbf{j}_{\mathbf{q}}\right]\cdot\hat{\mathcal{A}}^{-1}\mathbf{j}_{\mathbf{q}}-\left[\left(\frac{D(\omega_{\mathbf{q}})^2}{2\sigma(\omega_{\mathbf{q}})}\right)'\boldsymbol{\nabla}\omega_{\mathbf{q}}+\frac{D(\omega_{\mathbf{q}})^2}{\sigma(\omega_{\mathbf{q}})}\boldsymbol{\nabla}\right]\cdot\hat{\mathcal{A}}\boldsymbol{\nabla}\omega_{\mathbf{q}}+\frac{1}{2}\sigma'(\omega_{\mathbf{q}})\mathbf{E}\cdot\hat{\mathcal{A}}\mathbf{E}-\zeta=0 \tag{36}$$

$$D(\omega_{\mathbf{q}})\boldsymbol{\nabla}\omega_{\mathbf{q}}+\hat{\mathcal{A}}^{-1}\mathbf{j}_{\mathbf{q}}+\sigma(\omega_{\mathbf{q}})\left[\boldsymbol{\kappa}-\boldsymbol{\nabla}\Psi\right]=0\,, \tag{37}$$

$$\int_\Lambda d\mathbf{r}\left(\frac{\omega_{\mathbf{q}}-\rho_0}{\sigma(\omega_{\mathbf{q}})}\right)\hat{\mathcal{A}}^{-1}\mathbf{j}_{\mathbf{q}}=0\,, \tag{38}$$

where we have defined $\mathbf{j}_{\mathbf{q}}(\mathbf{r}) \equiv \mathbf{q}-\mathbf{v}_{\mathbf{q}}\left[\rho_0-\omega_{\mathbf{q}}(\mathbf{r})\right]+\boldsymbol{\phi}_{\mathbf{q}}(\mathbf{r})$ for simplicity in notation.

As discussed above, our local stability analysis shows that whenever the transition is unleashed, the leading instability is a density wave with structure in one dimension only, determined either by the minimum-anisotropy direction, see condition (iii) above, or by the orientation of the current vector for isotropic systems, see (iv). Such a $1d$ traveling wave will dominate the optimal solution of our variational problem *at least* in a finite region below the transition line, so we now assume $1d$ optimal traveling-wave fields of the form $\omega_{\mathbf{q}}(x_\parallel)$ and $\boldsymbol{\phi}_{\mathbf{q}}(x_\parallel)$ (recall that we denote as $x_\parallel$ the direction of structure formation, and $x_\perp$ the orthogonal, structureless direction). Next we decompose the optimal vector field $\boldsymbol{\phi}_{\mathbf{q}}$ along the $\parallel$- and $\perp$-directions, $\boldsymbol{\phi}_{\mathbf{q}}(x_\parallel) = [\phi^{\parallel}_{\mathbf{q}}(x_\parallel),\phi^{\perp}_{\mathbf{q}}(x_\parallel)]$. The divergence-free constraint (33) on $\boldsymbol{\phi}_{\mathbf{q}}(x_\parallel)$ immediately implies that $\phi^{\parallel}_{\mathbf{q}}$ is in fact a constant, while the zero-integral constraint (32) sets this constant to zero, resulting in a simplfied form of the vector field $\boldsymbol{\phi}_{\mathbf{q}}(x_\parallel) = [0,\phi^{\perp}_{\mathbf{q}}(x_\parallel)]$. This in turn implies that

$$j^{\parallel}_{\mathbf{q}}(x_\parallel) = q_\parallel - v_\parallel[\rho_0-\omega_{\mathbf{q}}(x_\parallel)]\,. \tag{39}$$

Now, by differentiating the $\perp$-component of Eq. (37) with respect to $x_\perp$, it is straightforward to see that $\partial_\perp\Psi$ is a function of $x_\parallel$ at most. Moreover, doing the same differentiation on the $\parallel$-component of (37), we obtain that $\partial_\parallel\partial_\perp\Psi=0$, which together with the previous observation implies that $\partial_\perp\Psi$ is indeed a constant. Using this information in the $\perp$-component of Eq. (37) together with constraint (8) on the empirical current, we obtain that

$$j^{\perp}_{\mathbf{q}}(x_\parallel) = q_\perp\frac{\sigma[\omega_{\mathbf{q}}(x_\parallel)]}{\int_0^1\sigma[\omega_{\mathbf{q}}(x_\parallel)]dx_\parallel}\,. \tag{40}$$

We next focus on Eq. (36). Multiplying this equation by $\omega'_{\mathbf{q}}(x_\parallel)$, using that $dF[\omega_{\mathbf{q}}(x_\parallel)]/dx_\parallel = F'(\omega_{\mathbf{q}})\,\omega'_{\mathbf{q}}(x_\parallel)$ for any arbitrary functional $F(\omega_{\mathbf{q}})$, and the identity

$$\frac{d\mathbf{j}_{\mathbf{q}}(x_\parallel)}{dx_\parallel} = \mathbf{v}_{\mathbf{q}}\omega'_{\mathbf{q}}(x_\parallel) + \frac{d\boldsymbol{\phi}_{\mathbf{q}}(x_\parallel)}{dx_\parallel}\,, \tag{41}$$

Eq. (36) can be rewritten as

$$\frac{d}{dx_\parallel}\left[\frac{1}{2\sigma(\omega_{\mathbf{q}})}\mathbf{j}_{\mathbf{q}}\cdot\hat{\mathcal{A}}^{-1}\mathbf{j}_{\mathbf{q}} - a_{\min}\frac{D(\omega_{\mathbf{q}})^2}{2\sigma(\omega_{\mathbf{q}})}\left(\frac{d\omega_{\mathbf{q}}}{dx_\parallel}\right)^2 + \frac{1}{2}\sigma(\omega_{\mathbf{q}})\mathbf{E}\cdot\hat{\mathcal{A}}\mathbf{E}\right] - \frac{1}{a_{\max}\sigma(\omega_{\mathbf{q}})}\frac{d\phi^\perp_{\mathbf{q}}(x_\parallel)}{dx_\parallel}j^\perp_{\mathbf{q}}(x_\parallel) - \zeta\omega'_{\mathbf{q}}(x_\parallel) = 0. \tag{42}$$

Integrating this equation once and taking into account the form of $j^\perp_{\mathbf{q}}(x_\parallel)$, see Eq. (40), we arrive at a differential equation for the optimal traveling-wave profile

$$X(\omega_{\mathbf{q}})\left(\frac{d\omega_{\mathbf{q}}}{dx_\parallel}\right)^2 - Y(\omega_{\mathbf{q}}) + \tilde{K}\omega_{\mathbf{q}}(x_\parallel) - K = 0\,, \tag{43}$$

with K and $\tilde{K}$ two constants which comprise the Lagrange multiplier ζ, the wave velocity $\mathbf{v}_{\mathbf{q}}$, and information on the boundary conditions, and where we have defined

$$X(\omega) \equiv \frac{D(\omega)^2}{2\sigma(\omega)}a_{\min}\,, \tag{44}$$

$$Y(\omega) \equiv \frac{\sigma(\omega)}{2}\left(\mathbf{E}\cdot\hat{\mathcal{A}}\mathbf{E} + \frac{[q_\parallel - v_\parallel(\rho_0-\omega)]^2}{a_{\min}\sigma(\omega)^2} - \frac{q_\perp^2}{a_{\max}(\int_0^1\sigma(\omega)dx_\parallel)^2}\right). \tag{45}$$

Finally, two additional equations follow from the $\parallel$-component of Eq. (38) and constraint (31)

$$\int_0^1 dx_\parallel \frac{[\omega_{\mathbf{q}}(x_\parallel)-\rho_0]}{a_{\min}\sigma(\omega_{\mathbf{q}})}\left[q_\parallel - v_\parallel(\rho_0-\omega_{\mathbf{q}}(x_\parallel))\right] = 0\,, \tag{46}$$

$$\rho_0 = \int_0^1 \omega_{\mathbf{q}}(x_\parallel)\,dx_\parallel\,, \tag{47}$$

which complete the system of coupled integro-differential equations for the optimal fields.

In order to solve this system, we now introduce a reparametrization which simplifies the numerical evaluation of the optimal $1d$ density wave profile and thus of the current LDF $G(\mathbf{q})$. First note that, in our geometry, Eq. (43) leads to a periodic optimal profile *symmetric* around $x_\parallel = 1/2$ (recall that $x_\parallel \in [0,1]$), i.e. with reflection symmetry $x_\parallel \to 1-x_\parallel$. Next we consider the possible maxima and minima of the optimal density wave. For models with a quadratic mobility transport coefficient $\sigma(\omega)$, as the WASEP and KMP models typically studied in literature, the number of possible maxima ω_+ and minima ω_- of the curve $\omega_{\mathbf{q}}(x_\parallel)$ is rather restricted, see Eq. (43) once particularized for $\omega'_{\mathbf{q}}(x_\parallel) = 0$. In the simplest case [3, 10], a single maximum $\omega_+ = \omega_{\mathbf{q}}(x^+_\parallel)$ and minimum $\omega_- = \omega_{\mathbf{q}}(x^-_\parallel)$ will appear, such that the position of two consecutive extrema $x^+_\parallel$ and $x^-_\parallel$ is such that $|x^+_\parallel(k) - x^-_\parallel(k)| = 1/2n$, with n the number of cycles in the unit interval. One can then study numerically the dependence of the current LDF on the number n of cycles, finding that $n=1$ is the optimal case. We hence restrict hereafter to $1d$ density waves with a single maximum and minimum with $n=1$. As a result, we can express now the constants $\tilde{K}$ and K of Eq. (43) in terms of these extrema

$$Y(\omega_\pm) = \tilde{K}\omega_\pm - K\,. \tag{48}$$

The values of these extrema $\omega_\pm$ can be obtained from the constraints on the distance between them and the total density of the system. In particular, the first constraint leads to the following equation,

$$1 = \int_0^1 dx_\parallel = 2\int_{\omega_-}^{\omega_+}\frac{d\omega_{\mathbf{q}}}{\omega'_{\mathbf{q}}} = 2\int_{\omega_-}^{\omega_+} f(\omega_{\mathbf{q}})\,d\omega_{\mathbf{q}} \tag{49}$$

with

$$f(\omega_{\mathbf{q}}) \equiv \sqrt{\frac{X(\omega_{\mathbf{q}})}{Y(\omega_{\mathbf{q}}) - \tilde{K}\omega_{\mathbf{q}} + K}} \tag{50}$$

as derived from Eq. (43), while the constraint on the total density leads to

$$\rho_0 = \int_0^1 \omega_{\mathbf{q}}(x_\parallel)\, dx_\parallel = 2\int_{\omega_-}^{\omega_+} \frac{\omega_{\mathbf{q}}}{\omega'_{\mathbf{q}}} d\omega_{\mathbf{q}} = 2\int_{\omega_-}^{\omega_+} \omega_{\mathbf{q}} f(\omega_{\mathbf{q}})\, d\omega_{\mathbf{q}}\,. \tag{51}$$

Note that the unknown variables $\omega_\pm$ appear as integration limits in Eqs. (49) and (51), difficulting the numerical solution of this problem. However, a suitable change of variables in ω-space allows to drop this dependence. In particular, we write now $\omega_{\mathbf{q}} \equiv \omega_- + \Omega(\omega_+ - \omega_-)$, with $\Omega \in [0,1]$, and define $h(\Omega) \equiv (\omega_+ - \omega_-) f[\omega_- + \Omega(\omega_+ - \omega_-)]$. With this choice, constraints (49) and (51), together with Eq. (46) for the velocity, now read

$$\frac{1}{2} = \int_0^1 h(\Omega)\, d\Omega\,, \tag{52}$$

$$\frac{\rho_0}{2} = \int_0^1 \omega_{\mathbf{q}}(\Omega) h(\Omega)\, d\Omega\,, \tag{53}$$

$$\int_0^1 h(\Omega) \frac{[\omega_{\mathbf{q}}(\Omega) - \rho_0]}{a_{\min}\sigma[\omega_{\mathbf{q}}(\Omega)]} \left[q_\parallel - v_\parallel(\rho_0 - \omega_{\mathbf{q}}(\Omega))\right]\, d\Omega = 0\,. \tag{54}$$

The solution of this three integral equations for a particular model and a given current vector $\mathbf{q}$ leads to particular values of the parameters ω_-, ω_+ and $v_\parallel$, which can be used in turn to obtain the constants K and $\tilde{K}$ from Eq. (48) needed to solve numerically the differential equation (43) for the optimal density wave profile [3, 10] and thus obtain the current LDF $G(\mathbf{q})$.

A related, interesting function is the dynamical free energy (dFE) $\mu(\boldsymbol{\lambda})$ discussed in the main text. This is nothing but the scaled cumulant generating function associated to the current probability distribution $P_\tau(\mathbf{q})$, defined as $\mu(\boldsymbol{\lambda}) \equiv \lim_{t\to\infty} t^{-1} \ln\langle e^{t\boldsymbol{\lambda}\cdot\mathbf{q}}\rangle$ or equivalently as the Legendre transform of the current LDF,

$$\mu(\boldsymbol{\lambda}) = \max_{\mathbf{q}}[G(\mathbf{q}) + \boldsymbol{\lambda}\cdot\mathbf{q}]\,, \tag{55}$$

with $\boldsymbol{\lambda}$ a vector conjugated to the current. This function can be seen as the conjugate *potential* to $G(\mathbf{q})$, a relation equivalent to the free energy being the Legendre transform of the internal energy in thermodynamics. The above MFT analysis of the dynamic phase transition can be developed also in terms of $\mu(\boldsymbol{\lambda})$, and this allows a direct comparison with the results of numerical experiments based on the cloning Monte Carlo method, see main text. In particular, defining $\mathbf{z} \equiv \boldsymbol{\lambda} + \mathbf{E}$, it can be shown that a line of critical values $\mathbf{z}_c$ exists at which the instability appears, defined by the equation $\mathbf{z}_c \cdot \hat{\mathcal{A}}\mathbf{z}_c = \Xi_c$, with Ξ_c the critical threshold defined in Eq. (21) above. This critical line separates a phase of Gaussian current statistics and homogeneous optimal profiles, corresponding to a quadratic dFE $\mu_{\rm G}(\mathbf{z}) = \sigma_0(\mathbf{z}\cdot\hat{\mathcal{A}}\mathbf{z} - \mathbf{E}\cdot\hat{\mathcal{A}}\mathbf{E})/2$, see Eq. (10), and the non-Gaussian, traveling-wave phase. As before, for systems with $\sigma_0'' > 0$ (as the KMP model) the Gaussian regime dominates for $\mathbf{z}\cdot\hat{\mathcal{A}}\mathbf{z} \le \Xi_c$ while the traveling-wave region appears for $\mathbf{z}\cdot\hat{\mathcal{A}}\mathbf{z} > \Xi_c$ and $\forall\mathbf{E}$. On the other hand, for systems with $\sigma_0'' < 0$ (as the WASEP studied here) a line of critical values of the external field exist, defined by Eq. (22), beyond which the instability appears, $\mathbf{E}\cdot\hat{\mathcal{A}}\mathbf{E} \ge |\Sigma_c|$. In this strong field case, Gaussian statistics are expected $\forall\mathbf{z}$ except for a region defined by $\mathbf{z}\cdot\hat{\mathcal{A}}\mathbf{z} \le \Xi_c$, where current fluctuations are non-Gaussian.

In this paper we are interested in the current statistics of the $2d$ anisotropic weakly asymmetric simple exclusion process (WASEP), see the main text. At the macroscopic level this model is defined by a diffusivity and mobility matrices $\hat{D}(\rho) = D(\rho)\hat{\mathcal{A}}$ and $\hat{\sigma}(\rho) = \sigma(\rho)\hat{\mathcal{A}}$, respectively, with $D(\rho) = 1/2$ and $\sigma(\rho) = \rho(1-\rho)$ (note that $\sigma''(\rho) < 0$). The diagonal anisotropy matrix $\hat{\mathcal{A}}$ has components $\hat{\mathcal{A}}_{\alpha\beta} = a_\alpha\delta_{\alpha\beta}$, with $\alpha,\beta = x$ or y. In particular, we consider systems such that $a_x = 1+\epsilon$ and $a_y = 1-\epsilon$, with ϵ an anisotropy parameter. The reason behind this choice is that, for finite lattice systems of moderate size L as the ones we can simulate effectively using the cloning method, a strong external field $\mathbf{E}$ induces an *effective* anisotropy in the medium, enhancing diffusivity and mobility along the field direction. This effect is modeled in our case, with $\mathbf{E}$ in the x-direction, with a parameter $\epsilon \ge 0$ so that the direction of minimum anisotropy (if any) is y. Using these definitions, one can particularize the previous theoretical

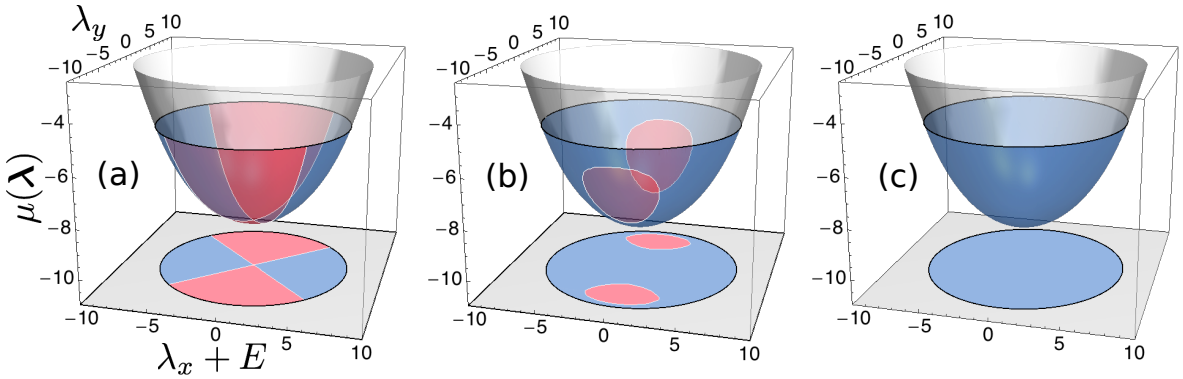

FIG. 1. (Color online) Dynamical free energy of the current for the $2d$-WASEP in an external field $\mathbf{E} = (10, 0)$ along the x-direction, as derived from MFT in the case of (a) no anisotropy, $\epsilon = 0$, (b) mild anisotropy, $0 < \epsilon < \epsilon_c$, and (c) strong anisotropy, $\epsilon > \epsilon_c$. A DPT appears between a Gaussian phase (light gray) with homogeneous optimal pathways, see sketch in Fig. 3.a representing a typical configuration trajectory in this case, and two different non-Gaussian symmetry-broken phases for low currents characterized by traveling-wave jammed states. The first DPT is 2^{nd}-order while the two symmetry-broken phases are separated by lines of 1^{st}-order DPTs, see Fig. 4 below.

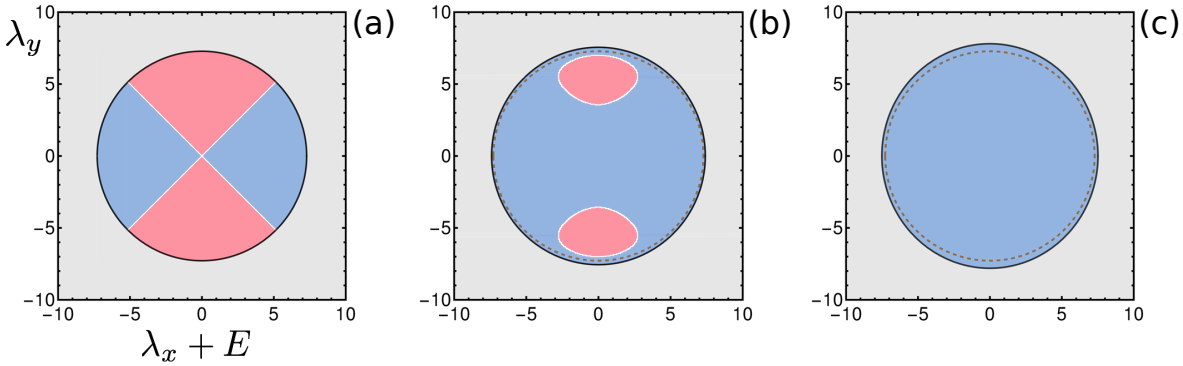

FIG. 2. (Color online) A closer look at the phase diagrams for current fluctuations in the case of (a) no anisotropy, $\epsilon = 0$, (b) mild anisotropy, $0 < \epsilon < \epsilon_c$, and (c) strong anisotropy, $\epsilon > \epsilon_c$, corresponding to the bottom projections in Fig. 1. The 2^{nd}-order DPT between the Gaussian phase (light gray) and the two different traveling-wave, non-Gaussian phases (dark blue and red) corresponds to the black thick line, while the 1^{st}-order DPT separating both symmetry-broken non-Gaussian phases is depicted as a white thin line. Panels (b) and (c) also include a dashed line which corresponds to the 2^{nd}-order DPT line for $\epsilon = 0$. This shows that the shape of this critical line does change as the anisotropy parameter ϵ increases.

framework for the $2d$ anisotropic WASEP and proceed to solve numerically the variational problem for the current dFE $\mu(\boldsymbol{\lambda})$ and the optimal profiles.

The solution of this problem shows that the interplay between the external field, the current and the anisotropy leads to a rich phase diagram for current fluctuations. Fig. 1 shows $\mu(\boldsymbol{\lambda})$, as derived from our MFT calculations, for three different values of the anisotropy ϵ. In all cases, the dynamic phase transition (DPT) between the Gaussian (light gray) and non-Gaussian (dark colors) phases appears for $\mathbf{z}_c \cdot \hat{\mathcal{A}}\mathbf{z}_c = \Xi_c$. Fig. 2 shows the phase diagrams for current fluctuations for the different anisotropy parameters (corresponding to the bottom projections of Fig. 1), and Fig. 3 shows raster plots sketching typical configuration trajectories for WASEP in the Gaussian current fluctuation phase, Fig. 3.a, and in the two different non-Gaussian symmetry-broken phases which appear for low currents, Figs. 3.b-c. In general, we find numerically that different traveling wave structures dominate different parts of the symmetry-broken, non-Gaussian phase, see Fig. 1. For isotropic systems, $\epsilon = 0$, the optimal density traveling wave for subcritical vectors $\mathbf{z} = (z_x, z_y)$ with $|z_x| > |z_y|$ ($|z_x| < |z_y|$) has structure along the y-direction (x-direction), preserving deep into the non-Gaussian phase the result derived from our local stability analysis right below the transition line, see item (iv) above. On the other hand, for anisotropic systems ($\epsilon > 0$) the transition triggers the formation of a density traveling wave with structure only along the minimum anisotropy, y-direction, see Figs. 1.b-c, 2.b-c and 3.b, in agreement with item (iii) above. However, for mild anisotropy we find deep into the non-Gaussian regime two pockets of the second symmetry-broken phase, i.e. the one with structure along the maximum anisotropy axis, see Figs. 1.b, 2.b and 3.c. These two patches decrease with increasing ϵ, up to a critical anisotropy $\epsilon_c \approx 0.035$ beyond which only the minimum-anisotropy density wave appears in the non-Gaussian regime, see Figs. 1.c and 2.c.

Next, we investigate the order of the different DPT's showing up in the current statistics of this model. We first

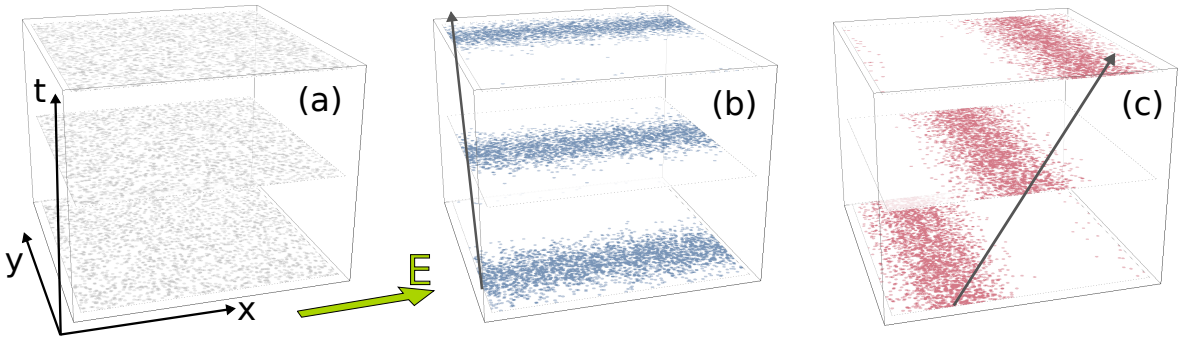

FIG. 3. (Color online) Raster plots of typical configuration trajectories for the anisotropic $2d$ WASEP in the Gaussian current fluctuation phase (a), and in the two different non-Gaussian symmetry-broken phases for low currents, (b) and (c), see also Fig. 1. These two novel phases are characterized by traveling density waves which jam particle flow along the field direction, (b) and blue phase in Fig. 1, or along the direction orthogonal to $\mathbf{E}$, (c) and red phase Fig. 1.

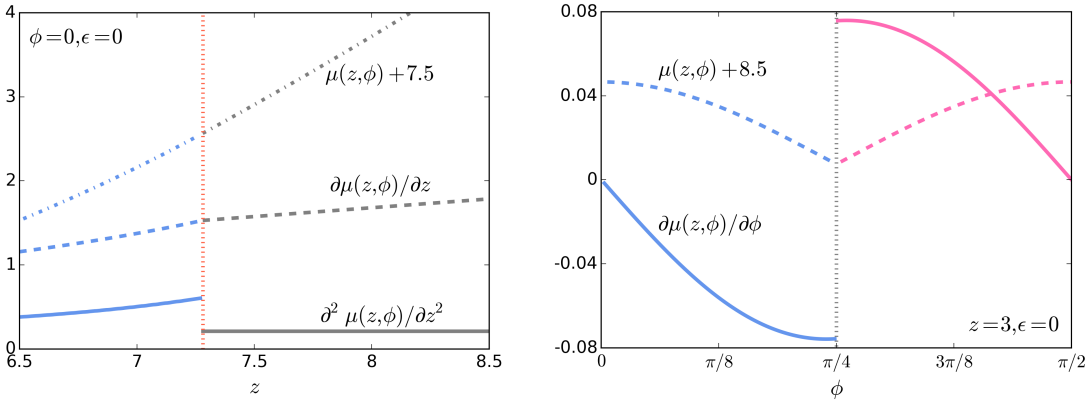

FIG. 4. (Color online) Left: Dynamical free energy for the current $\mu(z,\phi)$, with $\mathbf{z}=\boldsymbol{\lambda}+\mathbf{E}$, as a function of $z=|\mathbf{z}|$ for $\phi=0$ in the isotropic case ($\epsilon=0$), see Fig. 1.a, as well as its first and second partial derivative with respect to z. Note that $\mu(z,\phi)$ has been shifted vertically for the sake of clarity. The vertical dotted line signals the DPT between the Gaussian, homogeneous current fluctuation phase ($z>z_c(\phi)$) and the non-Gaussian, symmetry broken phase ($z<z_c(\phi)$) with jammed density waves along the field direction, see Fig. 3.b. The dynamical free energy exhibits a kink in its first derivative and an associated discontinuity in the second derivative, a hallmark of a second-order phase transition. Similar discontinuities in $\partial_z^2\mu(z,\phi)$ appear at $z_c(\phi)$ $\forall\phi\in[0,2\pi]$. Right: $\mu(z,\phi)$ vs ϕ for $\phi\in[0,\pi/2]$ and $z=3$ in the isotropic case ($\epsilon=0$), see Fig. 1.a, as well as its first derivative with respect to ϕ. As before, $\mu(z,\phi)$ has been shifted vertically for clarity. The vertical dotted line signals the DPT separating the two distinct non-Gaussian symmetry-broken phases with jammed states along the field direction ($\phi<\pi/4$) or orthogonal to it ($\phi>\pi/4$). While $\mu(z=3,\phi)$ is continuous across the transition, it exhibits a kink at $\phi_c=\pi/4$ and an associated discontinuity in $\partial_\phi\mu(z=3,\phi)$, signaling the first-order character of this DPT between the two symmetry-broken non-Gaussian phases.

focus on the DPT from the Gaussian to the non-Gaussian phase at $\mathbf{z}_c\cdot\hat{\mathcal{A}}\mathbf{z}_c=\Xi_c$. Left panel in Fig. 4 shows $\mu(\mathbf{z})$ as a function of $z=|\mathbf{z}|$ for a current angle $\phi=0$ in the isotropic case ($\epsilon=0$), as well as its first and second partial derivatives with respect to z at constant ϕ. Clearly, the dynamical free energy exhibits a kink in its first derivative and a related discontinuity in the second derivative, a hallmark of a second-order phase transition. Similar discontinuities in $\partial_z^2\mu(z,\phi)$ appear at $z_c(\phi)$ $\forall\phi\in[0,2\pi]$. Therefore, as happens also in the simpler DPT's already described and observed in $1d$ oversimplified transport models [10, 11], the DPT from the Gaussian, homogeneous phase and the non-Gaussian, traveling-wave phases is of second order type.

On the other hand, the DPT between different symmetry-broken phases for $\mathbf{z}_c\cdot\hat{\mathcal{A}}\mathbf{z}_c<\Xi_c$ and mild or no anisotropy, see Fig. 1.a-b, is clearly discontinuous. Indeed, right panel in Fig. 4 shows $\mu(\mathbf{z})$ as a function of the angle $\phi\in[0,\pi/2]$ for $z=3$ (deep into the symmetry-broken phase) in the isotropic case $\epsilon=0$, see Fig. 1.a, as well as its first derivative with respect to ϕ at constant z. The vertical dotted line in this plot signals the DPT separating the two distinct non-Gaussian symmetry-broken phases with traveling jammed states along the field direction ($\phi<\pi/4$) or orthogonal to it ($\phi>\pi/4$). While $\mu(z=3,\phi)$ is continuous across the transition, it exhibits a kink at $\phi_c=\pi/4$ and an associated discontinuity in $\partial_\phi\mu(z=3,\phi)$, signaling the first-order character of this DPT between the two symmetry-broken non-Gaussian phases. Something similar happens for all other subcritical z and $\epsilon<\epsilon_c$. Interestingly, along these 1^{st}-order DPT lines, both traveling wave solutions are equally probable, giving rise to a *coexistence* of two different

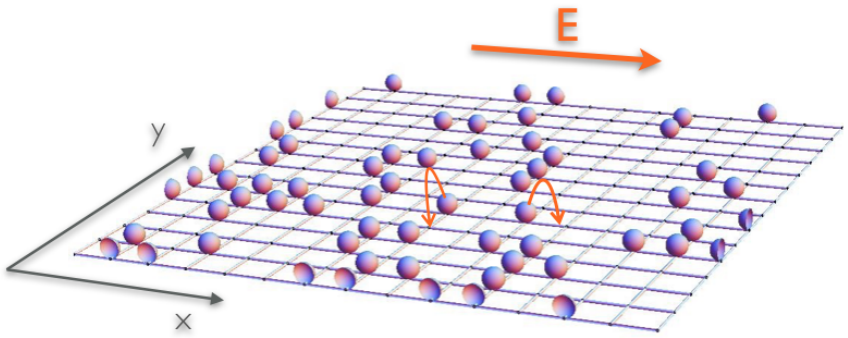

FIG. 5. (Color online) Sketch of the $2d$ weakly asymmetric simple exclusion process (WASEP). M particles evolve in a $2d$ square lattice of size $N = L \times L$ with periodic boundary conditions, such that $M \leq N$ and the global density is $\rho_0 = M/N$. Each site might be occupied by one particle at most, which jumps stochastically to neighboring empty sites at a rate $r^{\alpha}_{\pm} \equiv \exp[\pm E_\alpha/L]/2$ for moves along the $\pm\alpha$-direction, $\alpha = x, y$, with $\mathbf{E} = (E_x, E_y)$ the external field.

dynamic fluctuating phases very much reminiscent of standard first-order critical phenomena.

To end this section we note that, even though our local stability analysis shows that the dominant perturbations immediately beyond the instability line are one-dimensional traveling waves, in principle one could expect more complex two-dimensional (traveling-wave) patterns to emerge deeper into the symmetry-broken phase. In this case, the equations defining the form of the optimal profiles are partial differential equations, see e.g. Eq. (36), and the uniqueness of their solution is in general unknown. However, one can find some particular solutions which are *local* maximizers of the MFT action for currents. The particular $2d$ solutions we have explored numerically do not improve the current LDF when compared to their $1d$ counterparts described above. In any case, we cannot discard exotic $2d$ solutions not yet explored, though our simulation results in the main text strongly support that $1d$ traveling waves are the global optimal solutions in all cases.

II. AN ORDER PARAMETER FOR THE DYNAMIC PHASE TRANSITION

In this section we describe in more detail the novel order parameter introduced in the main text to detect and characterize the onset of the 2^{nd}-order DPT predicted by MFT. Let us first fix some notation. The $2d$-WASEP is defined at the microscopic level on a $2d$ square lattice of size $N = L \times L$ with periodic boundaries where $M \leq N$ particles evolve, so the global density is $\rho_0 = M/N$, see sketch in Fig. 5. Each lattice site may contain at most one particle, so the state of the system is defined by an occupation vector $\mathbf{n} \equiv \{n_{ij} = 0, 1; i, j \in [1, L]\}$, with $M = \sum_{i,j=1}^{L} n_{ij}$. Particles perform stochastic jumps to neighboring empty sites at a rate $r^{\alpha}_{\pm} \equiv \exp[\pm E_\alpha/L]/2$ for jumps along the $\pm\alpha$-direction, $\alpha = x, y$, with $\mathbf{E} = (E_x, E_y)$ the external field.

As described in the previous section, macroscopic fluctuation theory predicts a dynamic phase transition in the current statistics of this model, for currents well below the average. In particular, we expect order to emerge across the DPT in the form of $1d$ coherent traveling waves which jam particle flow along one direction, thus facilitating low-current deviations. The interplay described above among the external field, anisotropy and currents opens the door to different, competing symmetry-broken phases, see Figs. 1, 2 and 3, and our aim here is to determine which ones do emerge in our simulations. To define an appropriate order parameter we perform now a *tomographic analysis* by taking $1d$ sections of our $2d$ system. In particular we consider a microscopic particle configuration $\mathbf{n}$ and slice it along one of the principal axes, say x, defining the j-slice configuration $\mathbf{n}_j \equiv \{n_{ij}; i \in [1, L]\}$, with $M_j = \sum_{i=1}^{L} n_{ij}$ the total number of particles in this slice and $M = \sum_{j=1}^{L} M_j$, see e.g Figs. 6.a,d. To properly take into account the periodic boundaries (i.e. the system torus topology, see Figs. 6.b,e), we consider each j-slice as a $1d$ ring of fixed radius embedded in $2d$ where each site $i \in [1, L]$ is assigned an angle $\theta_i = 2\pi i/L$, and compute the angular position of the center of mass for the j-slice, $\theta^{(j)}_{\text{cm}}$. This is defined as

$$\theta^{(j)}_{\text{cm}} \equiv \tan^{-1}\left(\frac{S_j}{C_j}\right) \tag{56}$$

with the additional definitions

$$S_j \equiv \frac{1}{M_j} \sum_{i=1}^{L} n_{ij} \sin\theta_i \,, \tag{57}$$

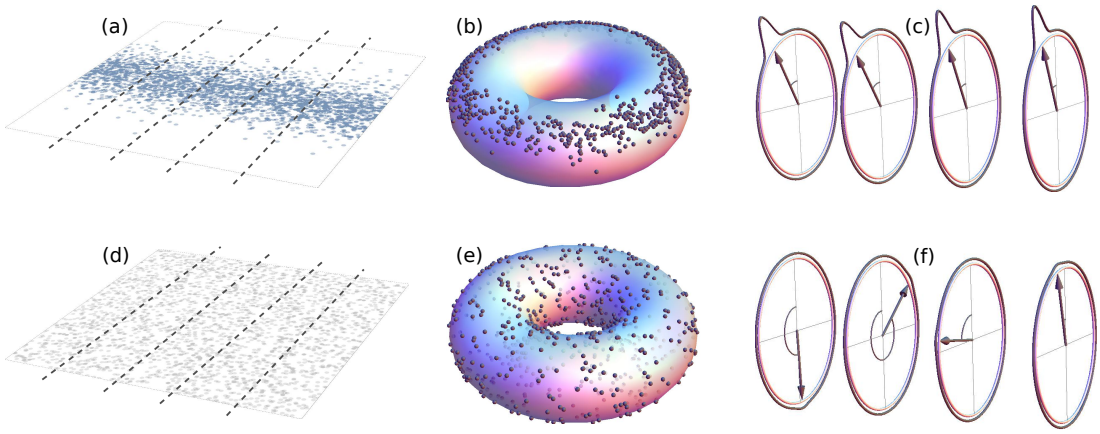

FIG. 6. (Color online) Tomographic analysis to define an order parameter for the DPT. Order is expected to emerge across the DPT in the form of $1d$ coherent traveling waves (a) which jam particle flow along one direction. To detect these jams, we slice microscopic configurations along principal axes (see dashed lines in (a)). Due to the periodic boundaries, the systems topology is in fact that of a torus, as in (b), so each slice can be considered as a 1d ring of fixed radius embedded in 2d, with a given angular mass distribution (c) depending on the positions of the particles in the slice. A small dispersion σ_x^2 of the angular centers of mass across the different slices, (c), will signal the formation of a coherent jam along the x-direction and the associated density wave in the orthogonal direction, see (a). A similar analysis in the homogeneous, Gaussian phase leads to a typically large dispersion σ_x^2, see (d)-(f).

$$C_j \equiv \frac{1}{M_j}\sum_{i=1}^{L} n_{ij}\cos\theta_i\,. \tag{58}$$

Clearly, a small dispersion of the angular centers of mass across the different slices will signal the formation of a coherent jam along the x-direction and the associated density wave in the orthogonal direction, see Fig. 6.c. On the other hand, a large dispersion of $\theta_{\rm cm}^{(j)}$ across the different $j \in [1, L]$ is the typical signature of a structureless, homogeneous random configuration, see Figs. 6.d,f. In this way, we write

$$\sigma_x^2 \equiv \langle(\theta_{\rm cm}^{(j)})^2\rangle_x - \langle\theta_{\rm cm}^{(j)}\rangle_x^2\,, \tag{59}$$

where we have defined

$$\langle f_j\rangle_x \equiv \frac{1}{L}\sum_{j=1}^{L} f_j\,, \tag{60}$$

for any arbitrary local observable f_j, and define the *tomographic x-coherence* as

$$\Delta_x(\boldsymbol{\lambda}) \equiv 1 - \langle\sigma_x^2\rangle_{\boldsymbol{\lambda}}\,, \tag{61}$$

where the average $\langle\cdot\rangle_{\boldsymbol{\lambda}}$ is taken over the biased $\boldsymbol{\lambda}$-ensemble, i.e. over all trajectories statistically relevant for a rare event of fixed $\boldsymbol{\lambda}$ [2, 3, 9]. We can define in an equivalent way the tomographic y-coherence $\Delta_y(\boldsymbol{\lambda})$ to detect particle jams along the y-direction, and Fig. 3.d in the main text shows these two order parameters measured across the DPT as a function of $z = |\mathbf{z}|$, with $\mathbf{z} \equiv \boldsymbol{\lambda} + \mathbf{E}$.

Remarkably, $\Delta_x(z)$ increases steeply for $\mathbf{z}\cdot\hat{\mathcal{A}}\mathbf{z} \leq \Xi_c$ and *all angles* ϕ of the current vector, while $\Delta_y(z)$ remains small and does not change appreciably across the DPT, clearly indicating that a coherent particle jam emerges along the x-direction in all cases, as in the sketch of Fig. 6.a above. This means that only one of the two possible symmetry-broken phases appear in our simulations (regardless of the current vector orientation), as expected from MFT in the supercritical anisotropy regime $\epsilon > \epsilon_c$, see Fig. 1.c, and consistent with the measured effective anisotropy $\epsilon \approx 0.038 > \epsilon_c$, see inset in Fig. 3.d of the main text. Note also that the behavior of both Δ_α ($\alpha = x, y$) across the DPT is consistent with the emergence of a traveling wave with structure in $1d$ and not in $2d$, as in the latter case both Δ_α should increase upon crossing $z_c(\phi)$. Moreover, the acute but continuous change of $\Delta_x(\mathbf{z})$ across the DPT is consistent with a second-order transition, in agreement with the MFT prediction.

[1] L. Bertini, A. De Sole, D. Gabrielli, G. Jona-Lasinio and C. Landim, "Macroscopic fluctuation theory," Rev. Mod. Phys. **87**, 593 (2015).

[2] B. Derrida, "Non-equilibrium steady states: fluctuations and large deviations of the density and of the current," J. Stat. Mech. P07023 (2007).
[3] P. I. Hurtado, C. Pérez-Espigares, J. J. del Pozo, and P. L. Garrido, "Thermodynamics of currents in nonequilibrium diffusive systems: theory and simulation," J. Stat. Phys. **154**, 214 (2014).
[4] P. I. Hurtado, C. Pérez-Espigares, J. J. del Pozo, and P. L. Garrido, "Symmetries in fluctuations far from equilibrium," Proc. Natl. Acad. Sci. USA **108**, 7704 (2011).
[5] R. Villavicencio-Sánchez, R. J. Harris, and H. Touchette, "Fluctuation relations for anisotropic systems," Europhys. Lett. **105**, 30009 (2014).
[6] C. Pérez-Espigares, F. Redig, and C. Giardinà, "Spatial fluctuation theorem," J. Phys. A **48**, 35FT01 (2015).
[7] C. Kipnis, C. Marchioro and E. Presutti, "Heat flow in an exactly solvable model," J. Stat. Phys. **27**, 65 (1982).
[8] B. Derrida, "An exactly soluble non-equilibrium system: The asymmetric simple exclusion process, Phys. Rep. **301**, 65 (1998).
[9] T. Bodineau and B. Derrida, "Distribution of current in nonequilibrium diffusive systems and phase transitions, Phys. Rev. E **72**, 066110 (2005).
[10] C. Pérez-Espigares, P. L. Garrido, and P. I. Hurtado, "Dynamical phase transition for current statistics in a simple driven diffusive system," Phys. Rev. E **87**, 032115 (2013).
[11] P. I. Hurtado and P. L. Garrido, "Spontaneous symmetry breaking at the fluctuating level," Phys. Rev. Lett. **107**, 180601 (2011).